ACS central science

Research Article

Cite This: ACS Cent. Sci. 2019, 5, 349−356

http://pubs.acs.org/journal/acscii

Red Room-Temperature Phosphorescence of CDs@Zeolite Composites Triggered by Heteroatoms in Zeolite Frameworks

Bolun Wang,[†] Ying Mu,[‡] Hongyue Zhang,[†] Huaizhong Shi,[†] Guangrui Chen,[†] Yue Yu,[†] Ziqi Yang,[†] Jiyang Li,*[,†] and Jihong Yu*[,†,§]

[†]State Key Laboratory of Inorganic Synthesis and Preparative Chemistry, College of Chemistry, Jilin University, Changchun 130012, P. R. China

[‡]College of Chemistry and Chemical Engineering, Qingdao University, Shandong 266071, P. R. China

[§]International Center of Future Science, Jilin University, 2699 Qianjin Street, Changchun 130012, P. R. China

Supporting Information

ABSTRACT: Carbon dots (CDs) with red-emitting room-temperature phosphorescence (RTP) are rarely reported because of the increasing nonradiative decay of the excited states and the decreasing energy gap between the excited states and ground states. Herein, we demonstrate a facile strategy for modulating the RTP properties of CDs in terms of donor−acceptor energy transfer (EnT) in the CDs-in-zeolite system. Upon tuning of the heteroatoms (Zn^{2+}, Mn^{2+}) doped in the aluminophosphate zeolite frameworks, CDs@zeolite composites with green and red phosphorescence have been prepared via in situ hydrothermal synthesis. In such composites, the zeolite matrix provides an efficient confinement role in stabilizing the triplet states of CDs. Significantly, the Mn-doped zeolite could act as an energy acceptor allowing EnT from excitons of CDs to the dopant in the host matrix, generating the intriguing red RTP behavior. This work provides an effective strategy for developing CD-based composite materials with special RTP emissions as well as new fields for applications.

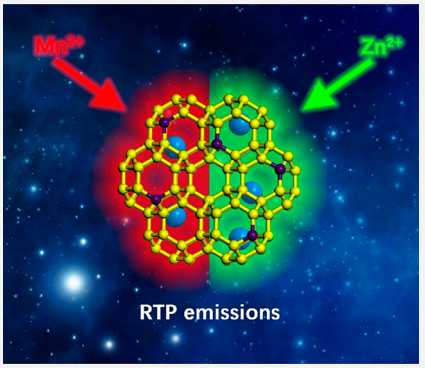

INTRODUCTION

Carbon dots (CDs), emerging as a new class of luminescent nanomaterials, have found potential applications of biological, optoelectronic, and energy-related fields for their unique optical properties, excellent biocompatibility, and easy preparation.[1−8] Particularly, phosphorescent CDs have shown more advantages over fluorescent CDs in the applications of bioelectronics and optoelectronics because phosphorescence that involves singlet-to-triplet intersystem crossing (ISC) makes its lifetimes and Stokes's shift usually longer and larger than those of fluorescence.[9−13] However, the room-temperature phosphorescence (RTP) of CDs is difficult to achieve because of the spin-forbidden nature of triplet exciton transitions and the predominance of accessible thermal decay pathways. Generally, the suppression of the nonradiative decay process and effective ISC from singlet to triplet states are required for RTP of CDs. To this end, several strategies including doping of N and P elements into CDs, increasing interactions between CDs (e.g., formation of hydrogen bonds, cross-link-enhanced emission), self-immobilizing excited triplet species, and embedding CDs in a solid matrix (e.g., poly(vinyl alcohol), potash alum, nanoporous materials, etc.) have been adopted to promote the generation of RTP of CDs.[14−21] It is noted that CDs with red-emitting RTP are rarely reported, which are highly desirable in in vivo imaging and light-emitting diodes. So far, red phosphorescent materials are mainly limited to organic compounds and rare earth metal complexes.[22−27] For organic molecules, narrowing the energy gap between the excited states and ground states is crucial in the design of RTP with red emission.[23,27] Particularly, the energy transfer (EnT) in the donor−acceptor (DA) system has proven to be effective for lowing the energy gap of transition-metal complexes.[28−31] This strategy might be feasible for CD-based composite materials. Recently, our research group developed a dots-in-zeolites strategy to prepare CD-based composites with fascinating thermally activated delay fluorescence properties with ultralong lifetimes.[32] This strategy provides a considerable flexibility to modulate the afterglow emissions of CDs by tuning the host matrix and the CD precursors. In the composites, the host zeolites could efficiently stabilize the triplet excited states by restricting the vibration and rotation of CDs. It is expected that the zeolite matrix may also serve as a suitable donor or acceptor to facilitate the EnT, thus promoting the red-emitting RTP property.

In this work, we demonstrate a facile strategy to modulate the RTP properties of composites by introducing heteroatoms into aluminophosphate zeolite frameworks to construct an efficient DA system and promote the exchange coupling between exciton of CDs and dopant in the host matrix. CDs@

Received: November 15, 2018
Published: January 22, 2019

DOI: 10.1021/acscentsci.8b00844
ACS Cent. Sci. 2019, 5, 349−356

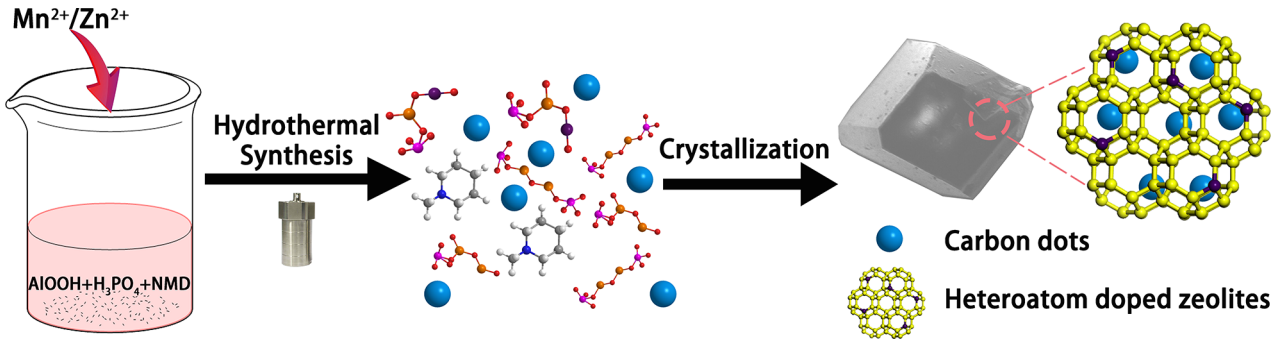

Figure 1. Schematic diagram for the formation process of CDs@zeolite composites. Introducing heteroatoms Zn or Mn into the reaction gel of aluminophosphate zeolite, the in situ formed CDs in the mother liquid are embedded into the zeolite matrix under hydrothermal conditions forming CD-based RTP materials with green or red emissions.

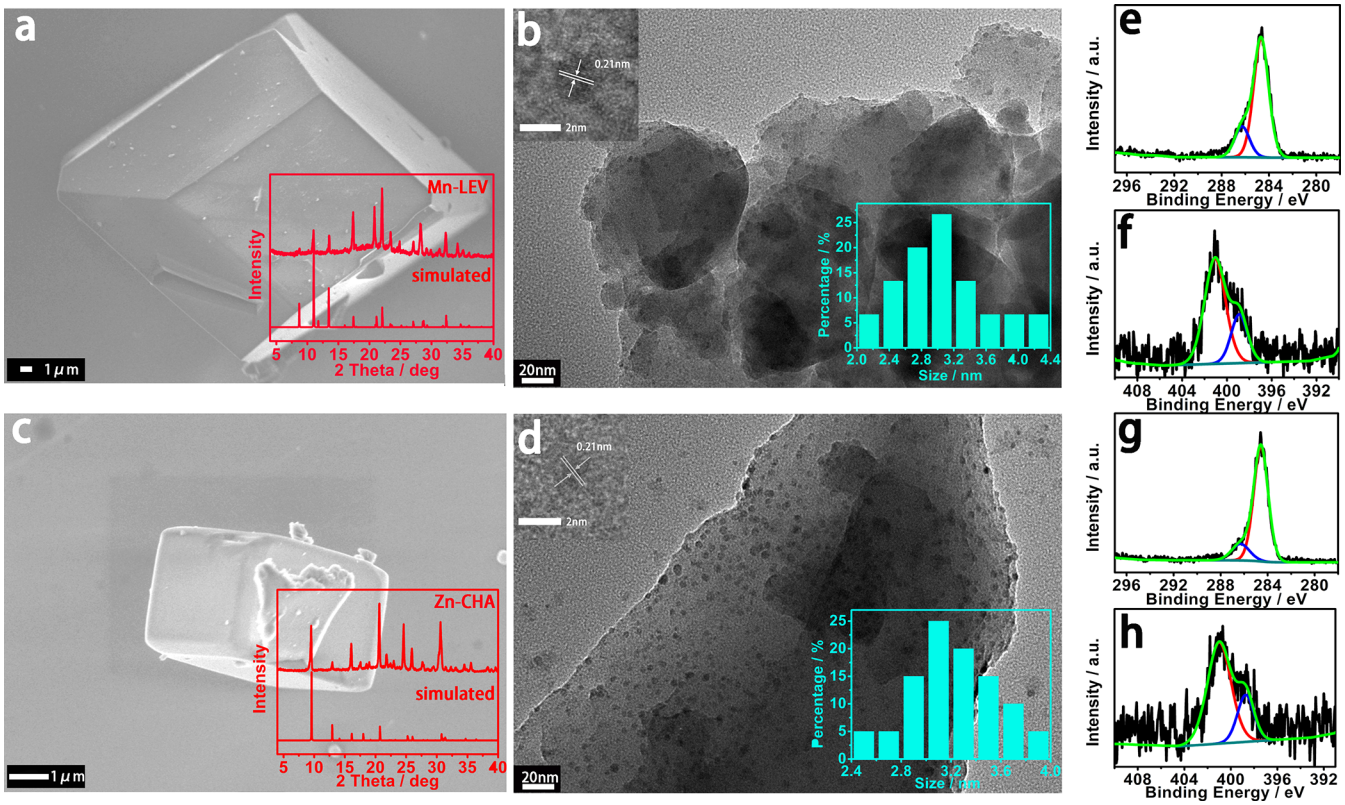

Figure 2. SEM, TEM images, and XPS spectra of CDs@Mn-LEV and CDs@Zn-CHA composites. (a, c) SEM images of CDs@Mn-LEV and CDs@Zn-CHA (inset: XRD patterns). (b, d) TEM images of CDs@Mn-LEV and CDs@Zn-CHA, showing CDs embedded in the zeolite matrix (inset: HRTEM images of CDs with lattice spacings of 0.21 nm (left) and size distributions of CDs (right) in two composites). (e, g) C 1s XPS spectra and (f, h) N 1s XPS spectra of CDs@Mn-LEV and CDs@Zn-CHA, respectively.

zeolite composites with green and red emissions have been successfully prepared in the hydrothermal synthetic system. Remarkably, the incorporation of Mn atoms in LEV zeolite affords EnT between CDs and the zeolite matrix, giving rise to a CD-based RTP material with red emission. The design concept presented in this work will open a new perspective for the RTP modulation of CD-based composite materials and inspire their further applications.

RESULTS AND DISCUSSION

Figure 1 illustrates the method to prepare CDs@zeolite composites with green or red RTP by in situ embedding CDs into a heteroatom-doped zeolite matrix under hydrothermal conditions. Typically, upon the choice of Mn and Zn as heteroatoms and *N*-methylpiperidine (NMD) as organic template, the composites are prepared in the reaction system of $MnO/ZnO-Al_2O_3-P_2O_5-NMD-H_2O$ at 180 °C for 3 days. The variation of heteroatoms in a similar gel system results in the formation of different zeolite types. As shown in Figure 2a,c, the Mn-doped zeolite crystals show a cuboid-like morphology, and the powder X-ray diffraction (XRD) pattern shows the characteristic LEV zeotype (denoted Mn-LEV), while the Zn-doped zeolite crystals exhibit the CHA zeotype with cubic morphology (denoted Zn-CHA). Inductive coupled plasma emission spectrometry (ICP) analysis together with energy-dispersive spectroscopy (EDS) spectra (Figure S1) give the M/Al molar ratio of 1/2 for both zeolites, and the organic template NMD molecules keep intact in their structures as

DOI: 10.1021/acscentsci.8b00844
ACS Cent. Sci. 2019, 5, 349−356

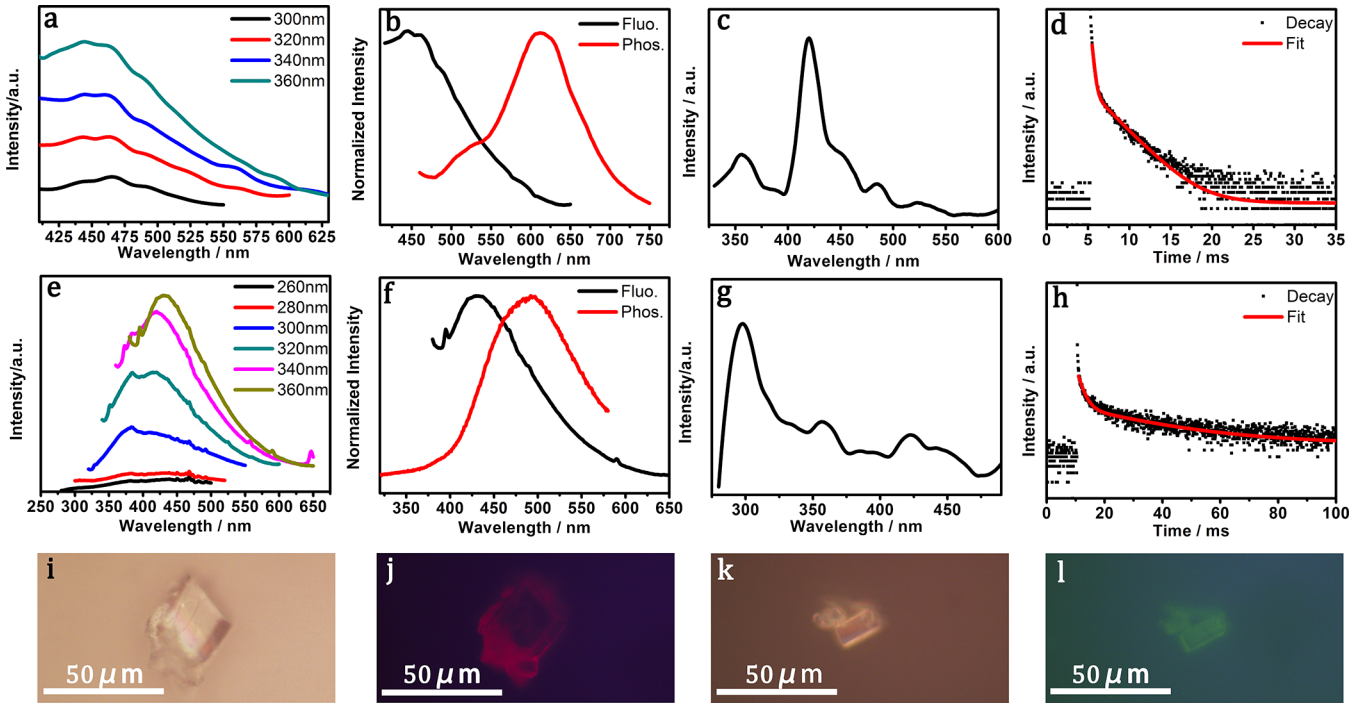

Figure 3. Photoluminescence properties of CDs@Mn-LEV and CDs@Zn-CHA composites. (a, e) Fluorescence emission spectra of CDs@Mn-LEV and CDs@Zn-CHA under different excitation wavelengths. (b, f) Normalized fluorescence (black line) and phosphorescence (red line) spectra of CDs@Mn-LEV and CDs@Zn-CHA. (c, g) Phosphorescence excitation spectra of CDs@Mn-LEV (λ_{em} = 620 nm) and CDs@Zn-CHA (λ_{em} = 500 nm). (d, h) Time-resolved phosphorescence decay and the corresponding fitting curves of CDs@Mn-LEV and CDs@Zn-CHA under 420 and 300 nm excitation, respectively. (i, j) Fluorescence microscopy images taken under white light exposure and excitation of green light with sample of CDs@Mn-LEV. (k, l) Fluorescence microscopy images under white light exposure and excitation of blue light with sample of CDs@Zn-CHA.

confirmed by liquid chromatography−high-resolution mass spectrometry (LC−HRMS) (Figure S2). TEM and SEM mappings also prove the existence of heteroatoms Mn or Zn in the zeolite matrices (Figures S1 and S3). The transmission electron microscopy (TEM) shows that CDs are embedded in the two crystalline zeolite matrices, and their average particle diameters are about 3.1−3.2 nm (Figure 2b,d). High-resolution TEM (HRTEM) images reveal that CDs in these two composites both have crystalline sp^2 domain with lattice spacing of 0.21 nm (insets of Figure 2b,d).[33,34] In residual mother solutions of CDs@Mn-LEV and CDs@Zn-CHA, CDs with a slightly smaller diameter of about 2.7−3.0 nm have also been clearly observed (Figure S4a,b). This indicates that CDs are simultaneously generated from the NMD precursor and then are embedded into the growing crystals of zeolites in the hydrothermal system, giving rise to the CDs@zeolite composites.

Interestingly, a photoluminescence (PL) property study reveals that CDs@Mn-LEV exhibits excitation-independent fluorescence with a broad emission centered at 460 nm. CDs@Zn-CHA shows excitation-dependent fluorescence with emission peaks varied from 375 to 430 nm (Figure 3a,e). When excited at 360 nm, CDs@Zn-CHA shows the strongest emission at 430 nm. In comparison, the diluted mother liquids of CDs@Mn-LEV and CDs@Zn-CHA both display excitation-dependent fluorescence (Figure S4c,d), which are similar to that of CDs@Zn-CHA.

The RTP performance including normalized fluorescence and phosphorescence spectra of the two composites has been studied. As shown in Figure 3b,f, when excited at 360 nm, CDs@Mn-LEV exhibits a major red phosphorescence emission at 620 nm, which presents a 160 nm red-shift compared to the fluorescence emission. In addition, a small shoulder peak of phosphorescence could be observed at about 500 nm. As for CDs@Zn-CHA, when excited at 360 nm the green phosphorescence is emitted at 500 nm, showing a 70 nm red-shift compared to the fluorescence. The RTP emissions of CDs@Mn-LEV and CDs@Zn-CHA give Commission Internationale de l'Eclairage (CIE) coordinates of (0.42, 0.40) and (0.18, 0.32), respectively (Figure S5). Figure 3c,g shows that the best phosphorescence excitation wavelengths of CDs@Mn-LEV and CDs@Zn-CHA are also different, which are 420 and 300 nm, respectively. The experimental and fitted phosphorescence lifetime decay curves show that CDs@Mn-LEV has an average lifetime of 1.81 ms, while CDs@Zn-CHA has a much longer lifetime of 22.32 ms (Figure 3d,h and Table S1). The phosphorescent quantum yields are 5.7% for CDs@Mn-LEV and 14.1% for CDs@Zn-CHA. Unfortunately, the phosphorescence of these two composites cannot be observed by the naked eye because of the transitory lifetime, but it still could be recognized under the fluorescence microscopy (Figure 3i−l).

For insight into the different RTP behaviors of CDs@Mn-LEV and CDs@Zn-CHA, the structures of CDs in the composites as well as in mother solutions have been studied. X-ray photoelectron spectroscopy (XPS) spectra show the presence of C—C/C=C (284.6 eV), C—N (286.0 eV), and N—H (401.1 eV)[35] bonds that may mainly correspond to the template NMD, and the additional C—N=C bonds (399.0 eV) should be related to CDs in these two composites (Figure 2e−h). UV−vis absorption and Fourier transform infrared (FTIR) spectra of the mother solutions of two composites are also similar, in which the $\pi-\pi^*$ transitions of C=C bonds

DOI: 10.1021/acscentsci.8b00844
ACS Cent. Sci. 2019, 5, 349−356

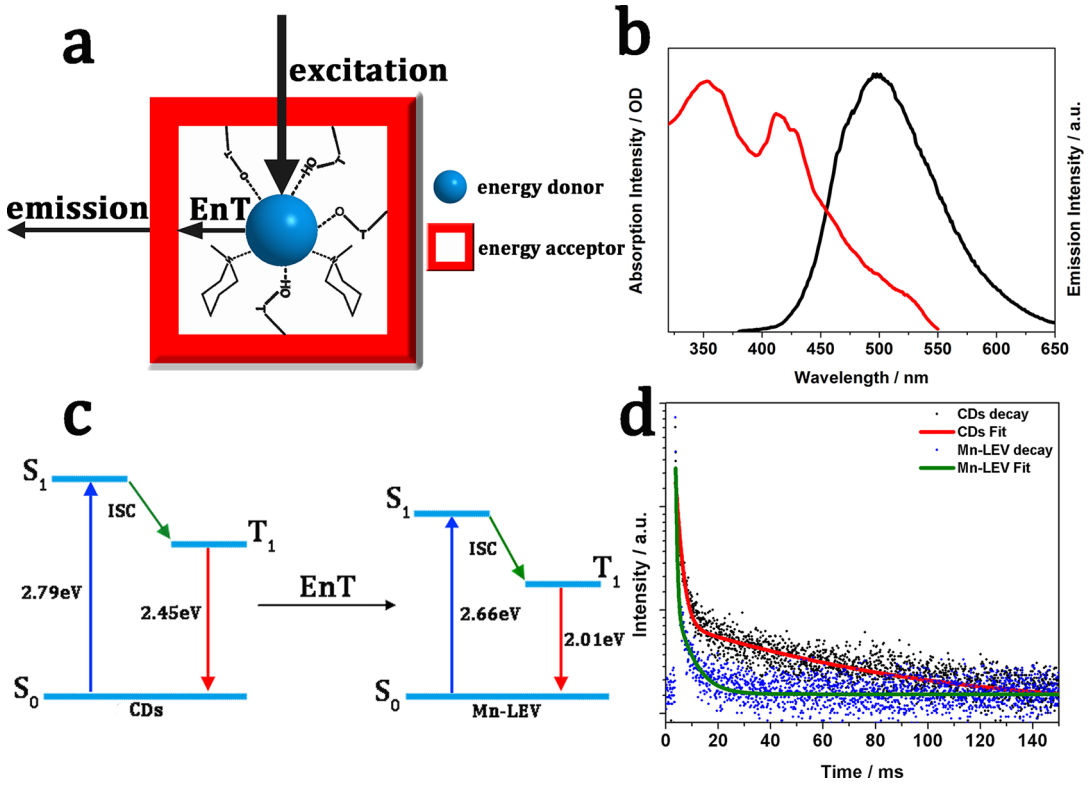

Figure 4. Proposed mechanism for CDs@Mn-LEV composites and the EnT process between CDs and the zeolite matrix. (a) Schematic of CDs confined in Mn-LEV zeolite. The CDs are well-stabilized by hydrogen bonds of the framework and templates. Meanwhile CDs and Mn-LEV zeolite serve as the energy donor and acceptor in the EnT process, respectively. (b) UV−vis absorption spectrum (red) of the Mn-LEV framework and emission spectrum (black) of CDs. (c) Energy diagram of CDs and Mn-LEV. The triplet energy (T_1) is determined by the phosphorescence emission maximum (505 and 616 nm for CDs and CDs@Mn-LEV, respectively). The singlet energy (S_1) is determined by the fluorescence emission maximum (444 and 460 nm for CDs and CDs@Mn-LEV, respectively). ISC: intersystem crossing. EnT: energy transfer. (d) Lifetime decays of the CDs (black, 77 K) and CDs@Mn-LEV (red, 77 K) at 500 nm. The spectra were recorded upon excitation at 360 nm.

(280 nm) of CDs can be obviously identified in UV−vis absorption spectra,[36−38] as well as C—N and N—H bonds which can be identified in FTIR spectra (Figure S6).[39−41] With the similar structure and PL properties of CDs in the mother solutions taken into account, it is presumed that the CDs embedded in both zeolite matrices are similar. Then, the role of the heteroatom-doped zeolite matrix in affecting the RTP properties of CDs@zeolite composites has been further investigated. Their FTIR spectra are similar (Figure S7b), while an obvious difference can be found in UV−vis absorption spectra of CDs@Mn-LEV and CDs@Zn-CHA: two new peaks located at 350 and 420 nm are identified in CDs@Mn-LEV (Figure S7a). Considering the similarity of CDs in two mother solutions, such new peaks in CDs@Mn-LEV are probably caused by Mn^{2+}-doped zeolite matrix.

For an understanding of the influence of heteroatoms and zeolite topologies on the RTP properties of CD-based materials, CDs@Zn-LEV has also been prepared by changing the molar ratio of Zn ions, H_2O, and NMD in the reaction gel (Figure S8a). The as-synthesized CDs@Zn-LEV has the same zeolite topology with CDs@Mn-LEV, but they exhibit distinct photoluminescence properties. CDs@Zn-LEV shows an excitation-dependent fluorescence from 360 to 470 nm with the best excitation wavelength of about 350 nm (Figure S8b). The green phosphorescence emission appears at 500 nm with the optimal excitation wavelength of 300 nm (Figure S8c,d). In fact, the luminescence property of CDs@Zn-LEV is similar to that of CDs@Zn-CHA. In addition, CDs in the mother solution of CDs@Zn-LEV have similar fluorescence emissions as compared to those observed in mother solutions of CDs@Mn-LEV and CDs@Zn-CHA (Figure S9). All the results confirm that the heteroatoms, but not zeolite topology, play a key role in regulating the RTP emissions of CDs@zeolite composites. The special red RTP behavior in CDs@Mn-LEV might be caused by the coupling of the Mn-doped matrix and CDs.

As for the RTP materials, it is important to obtain competent spin−orbit coupling for effectively populating triplet excitons through enhancing the ISC process and stabilizing triplet states. It is well-known that intramolecular vibrations and rotations can be suppressed in luminescence molecules at low temperature (77 K), which leads to more radiative transition and stable triplet states.[42] For unconfined CDs in mother solutions, no phosphorescence is observed at room temperature. At low temperature (77 K), with the mother solution of CDs@Mn-LEV taken as an example, it shows green phosphorescence emission with the best excitation wavelength located at 300 nm (Figure S10a,b) and a lifetime of 61.13 ms, which is quite similar to the green phosphorescence of CDs@Zn-CHA and CDs@Zn-LEV composites. This indicates that the green RTP of CDs@Zn-CHA and CDs@Zn-LEV primarily originates from the zeolite-confined CDs while the doped Zn atoms have no influence on the RTP performance. The nonradiative relaxation is effectively prevented by the steady matrix of zeolites with the confinement of emissive species and suppressing their

DOI: 10.1021/acscentsci.8b00844
ACS Cent. Sci. 2019, 5, 349−356

intramolecular rotations and vibrations, which leads to the stabilized triplet states of CDs. Such a confinement and stabilization effect of zeolite frameworks has already been studied before.[32]

In contrast, CDs@Mn-LEV emits red RTP, which is distinct from its mother solution that emits green RTP at 77 K. This indicates that the doped Mn atoms in zeolite might be responsible for the red RTP emission, and a possible EnT might occur between CDs to the Mn-doped LEV host matrix. As mentioned above, in the UV−vis adsorption spectrum of CDs@Mn-LEV (Figure S7a), there are two additional absorption peaks at 350 and 420 nm attributed to the Mn-LEV matrix. The good spectral overlap between the RTP emission of CDs and UV−vis absorbance of Mn-LEV may afford efficient EnT of photoinduced excitons from the CDs to the doped Mn in the host zeolite matrix (Figure 4a−c, Figure S11). Thus, it is believed that the red RTP emission of CDs@Mn-LEV comes from the transition ($4T_1$−$6A_1$) of Mn^{2+}, and the weak green RTP emission is due to the confined CDs. The similar mechanism of Mn^{2+}-related emission through the exciton energy transfer from the perovskite quantum dots to the doped Mn^{2+} ions has been widely reported previously.[43−46] Time-resolved phosphorescence measurements reveal a distinct decrease of lifetimes at 500 nm in CDs@Mn-LEV, compared to those of 77 K-CDs and CDs@Zn-CHA (Figure 4d, Table S2). This provides further evidence for the efficient donor−acceptor EnT in CDs@Mn-LEV.[47] The CDs@Mn-LEV exhibits a high EnT efficiency of 92.85% according to $\eta_{EnT} = 1 - \tau_{DA}/\tau_D$, and the EnT rate ($K_{EnT}$) is calculated to be 2.12×10^2 S^{-1} according to $K_{EnT} = 1/\tau_{DA} - 1/\tau_D$.[48−52] It is found that the amount of Mn atoms doped in LEV zeolite affects the emission intensity and lifetime of phosphorescence. For instance, upon an increase in the content of Mn from 8.19% to 13.42% (in weight), the emission intensity of RTP and average lifetime are slightly enhanced in CDs@Mn-LEV (Figure S12 and Table S3). Furthermore, it is believed that tuning the luminescent properties of confined CDs and the host matrix may further improve their energy transfer and thus enhance the RTP property of the composite materials. Some related works are ongoing.

The low-temperature phosphorescence emission spectrum of CDs@Mn-LEV is also helpful to prove the EnT process in the composite (Figure S13a). When excited at 420 nm (77 K), the red-emitting intensity at 620 nm decreases; meanwhile the green emission intensity at about 500 nm obviously increases. This suggests that the EnT process might be suppressed at low temperature, and therefore, CDs@Mn-LEV emits predominantly green phosphorescence at 77 K. At room temperature, the EnT process can be activated, and the red emission at 620 nm becomes predominant. As for CDs@Zn-CHA, however, green phosphorescence stays at 500 nm at room temperature and 77 K, revealing that no EnT process occurs in this composite (Figure S13b).

Notably, CDs@Mn-LEV with red RTP emission is quite stable under ultraviolet radiation or even atmosphere. The phosphorescence property remains for more than 3 h under a 30 W UV lamp (Figure S14a), and even more than 2 months at air condition (Figure S14b). This suggests that CDs@Mn-LEV can be used in atmosphere, and it is superior to most conventional organic RTP materials. In addition, the recyclable thermal-responsive phosphorescence emission of CDs@Mn-LEV from green to red upon heating up from 77 K to room temperature endows it potential applications as temperature sensors (Figure S15).

CONCLUSIONS

In summary, we have successfully constructed a donor−acceptor system by confining CDs in the heteroatom-doped zeolite matrices, which can efficiently tune the RTP behaviors of the resulting composites. The as-prepared CDs@Zn-CHA exhibits a green RTP with a lifetime of 22.32 ms, and CDs@Mn-LEV displays a predominant red RTP with a lifetime of 1.814 ms arising from the EnT process occurring between the Mn-doped zeolite matrix as acceptor and CDs as donor. Their phosphorescence quantum yields are 14.1% and 5.7%, respectively. In addition, the ultrastability of CDs@Mn-LEV in atmosphere as well as thermal-response phosphorescence emissions demonstrate the potential of these materials for further applications in light-emitting and temperature sensors. This work provides an effective strategy to the design and synthesis of novel CD-based RTP materials with modulated emissions (in particular red emission), which is promising for their future practical applications.

METHODS

Preparation of CDs@Mn-LEV. CDs@Mn-LEV was prepared under hydrothermal conditions in a reaction gel ratio of MnO−Al_2O_3−P_2O_5−*N*-methylpiperidine (NMD)−H_2O. Typically, 0.332 g of pseudoboehmite (Al_2O_3, 62.5%) and 0.5 g of manganese(II) acetate tetrahydrate ($Mn(CH_3COO)_2{\cdot}4H_2O$, 99.0%) were added into 14 mL of deionized water. Then, 0.6 mL of orthophosphoric acid (H_3PO_4, 85 wt %) was added into the solution with continuous stirring at room temperature. Next, 1.2 mL of NMD ($C_6H_{13}N$, 99.0%) was dropwise added to the reaction solution. The gel was further stirred for 2 h and crystallized at 180 °C in Teflon stainless-steel autoclaves for 72 h. The as-prepared zeolite was washed carefully and dried at 80 °C. The mother solution of CDs@Mn-LEV was collected for further experiments. The amount of Mn in the CDs@Mn-LEV composite could be modulated by adding $Mn(CH_3COO)_2{\cdot}4H_2O$ (99.0%) with different amounts (0.35, 0.40, 0.45, 0.55, 0.60, and 0.65 g) in the initial reaction system, and others kept unchanged. It was noted that the pure phase of Mn-LEV zeolite could not be obtained when the amount of $Mn(CH_3COO)_2{\cdot}4H_2O$ added was more than 0.65 g. In addition, the Mn-LEV zeolite without confined CDs also could not be synthesized in such a reaction system.

Preparation of CDs@Zn-CHA. CDs@Zn-CHA was synthesized in a similar hydrothermal system of ZnO−Al_2O_3−P_2O_5−*N*-methylpiperidine (NMD)−H_2O in which 0.448 g of zinc acetate dihydrate ($Zn(CH_3COO)_2{\cdot}2H_2O$, 99.0%) was used instead of 0.5 g of $Mn(CH_3COO)_2{\cdot}4H_2O$. The mother solution of CDs@Zn-CHA was also collected for further experiments.

Preparation of CDs@Zn-LEV. CDs@Zn-CHA was synthesized in hydrothermal conditions with a reaction gel system of ZnO−Al_2O_3−P_2O_5−*N*-methylpiperidine (NMD)−H_2O. Typically, 0.332 g of Al_2O_3 (62.5%) and 0.173 g of $Zn(CH_3COO)_2{\cdot}2H_2O$ (99.0%) were added into 10 mL of water, and 0.6 mL of H_3PO_4 (85 wt %) was further added into the solution with continuous stirring at room temperature. Then, 0.8 mL of NMD ($C_6H_{13}N$, 99.0%) was dropwise added to the reaction solution. The gel was further stirred for 2 h and

DOI: 10.1021/acscentsci.8b00844
ACS Cent. Sci. 2019, 5, 349−356

crystallized at 180 °C in Teflon stainless-steel autoclaves for 72 h. The as-prepared zeolite was washed carefully and dried at 80 °C. The mother solution of CDs@Zn-LEV was collected for further experiments.

Material Characterizations. The Rigaku Ultima IV diffractometer was used for collection of PXRD data with Cu Kα radiation (λ = 1.5418 Å). TEM, TEM mapping, HRTEM, and high-angle annular dark-field (HAADF) STEM images were recorded by using FEI Titan G2 60-300 scanning and an FEI Tecnai G2 S-Twin F20 instrument. SEM, SEM mapping, and EDS images were recorded by a JSM-6700F instrument. Bruker VERTEX 80/80v FTIR spectrometers were used for FTIR spectra with a background of potassium bromide. A Hitachi UV-2450 spectrophotometer and a Shimadzu U-4100 instrument were used for UV−vis adsorption spectra. The XPS measurements were measured by using a ThermoESCALAB250 spectrometer. LC−HRMS spectra were collected bya Bruker Agilent1290-micrOTOF Q II instrument. The deviation was not more than 3 mDa, and the mass spectra were calibrated by sodium acetate as an internal label.

Photoluminescence Measurements. A HORIBA Scientific Fluoromax-4P instrument is the spectrofluorometer for fluorescence and phosphorescence spectra measurements. A pulsed xenon lamp was used for phosphorescence spectra. The parameters of the phosphorescence measurement are listed as follows: 50 ms for sample window, 0.1 ms for delay after flash, 60 ms for time per flash, and 10 for flash count. The quantum yields were also measured by the HORIBA Scientific Fluoromax-4P instrument with an integrating sphere. An Olympus BX51 instrument was used for taking fluorescent images. The white, blue, and green light excitations went through band-pass filters at wavelengths of 550 and 580 nm.

Safety Statement. No unexpected or unusually high safety hazards were encountered.

■ ASSOCIATED CONTENT

Supporting Information

The Supporting Information is available free of charge on the ACS Publications website at DOI: 10.1021/acscentsci.8b00844.

Experimental details, further characterization, and figures including SEM mappings, EDS spectra, LC−HRMS results, TEM mappings, HAADF STEM images, particle diameter distributions, fluorescence emission spectra, CIE color coordinates, UV−vis absorption spectra, FTIR spectra, powder X-ray diffraction patterns, phosphorescence spectra, and phosphorescence intensity ratios (PDF)

■ AUTHOR INFORMATION

Corresponding Authors

*E-mail: lijiyang@jlu.edu.cn.
*E-mail: jihong@jlu.edu.cn.

ORCID

Yue Yu: 0000-0002-8189-8291
Jiyang Li: 0000-0002-5176-8939
Jihong Yu: 0000-0003-1615-5034

Notes

The authors declare no competing financial interest.

■ ACKNOWLEDGMENTS

We thank the National Natural Science Foundation of China (Grants 21671075, 21621001, 21835002) and the 111 Project (B17020) for financial support.

■ REFERENCES

(1) Zhu, S. J.; Meng, Q. N.; Wang, L.; Zhang, J. H.; Song, Y. B.; Jin, H.; Zhang, K.; Sun, H. C.; Wang, H. Y.; Yang, B. Highly Photoluminescent Carbon Dots for Multicolor Patterning, Sensors, and Bioimaging. *Angew. Chem., Int. Ed.* **2013**, *52*, 3953−3957.

(2) Miao, X.; Qu, D.; Yang, D. X.; Nie, B.; Zhao, Y. K.; Fan, H. Y.; Sun, Z. C. Synthesis of Carbon Dots with Multiple Color Emission by Controlled Graphitization and Surface Functionalization. *Adv. Mater.* **2018**, *30*, 1704740.

(3) Qu, D.; Liu, J.; Miao, X.; Han, M. M.; Zhang, H. C.; Cui, Z.; Sun, S. R.; Kang, Z. H.; Fan, H. Y.; Sun, Z. C. Peering into Water Splitting Mechanism of g-C_3N_4-carbon Dots Metal-free Photocatalyst. *Appl. Catal., B* **2018**, *227*, 418−424.

(4) Miao, X.; Yan, X. L.; Qu, D.; Li, D. B.; Tao, F. F.; Sun, Z. C. Red Emissive Sulfur, Nitrogen Codoped Carbon Dots and Their Application in Ion Detection and Theraonostics. *ACS Appl. Mater. Interfaces* **2017**, *9*, 18549−18556.

(5) Ding, H.; Yu, S. B.; Wei, J. S.; Xiong, H. M. Full-Color Light-Emitting Carbon Dots with a Surface-State-Controlled Luminescence Mechanism. *ACS Nano* **2016**, *10*, 484−491.

(6) Mu, Y.; Wang, N.; Sun, Z. C.; Wang, J.; Li, J. Y.; Yu, J. H. Carbogenic Nanodots Derived from Organo-templated Zeolites with Modulated Full-color Luminescence. *Chem. Sci.* **2016**, *7*, 3564−3568.

(7) Qu, S. N.; Wang, X. Y.; Lu, Q. P.; Liu, X. Y.; Wang, L. J. A Biocompatible Fluorescent Ink Based on Water-Soluble Luminescent Carbon Nanodots. *Angew. Chem., Int. Ed.* **2012**, *51*, 12215−12218.

(8) Kong, B.; Tang, J.; Zhang, Y. Y.; Jiang, T.; Gong, X. A.; Peng, C. X.; Wei, J.; Yang, J. P.; Wang, Y. C.; Wang, X. B.; Zheng, G. F.; Selomulya, C.; Zhao, D. Y. Incorporation of Well-Dispersed Sub-5-nm Graphitic Pencil Nanodots into Ordered Mesoporous Frameworks. *Nat. Chem.* **2016**, *8*, 171−178.

(9) Tao, S. Y.; Lu, S. Y.; Geng, Y. J.; Zhu, S. J.; Redfern, S. A. T.; Song, Y. B.; Feng, T. L.; Xu, W. Q.; Yang, B. Design of Metal-Free Polymer Carbon Dots: A New Class of Room-Temperature Phosphorescent Materials. *Angew. Chem., Int. Ed.* **2018**, *57*, 2393−2398.

(10) Mu, Y.; Shi, H. Z.; Wang, Y. F.; Ding, H.; Li, J. Y. CNDs@zeolite: New Room-temperature Phosphorescent Materials Derived by Pyrolysis of Organo-templated Zeolites. *J. Mater. Chem. C* **2017**, *5*, 10894−10899.

(11) Jiang, K.; Wang, Y. H.; Gao, X. L.; Cai, C. Z.; Lin, H. W. Facile, Quick, and Gram Scale Synthesis of Ultralong-Lifetime Room Temperature Phosphorescent Carbon Dots by Microwave Irradiation. *Angew. Chem., Int. Ed.* **2018**, *57*, 6216−6220.

(12) Hou, J.; Wang, L.; Zhang, P.; Xu, Y.; Ding, L. Facile Synthesis of Carbon Dots in An Immiscible System with Excitation-independent Emission and Thermally Activated Delayed Fluorescence. *Chem. Commun.* **2015**, *51*, 17768−17771.

(13) Jiang, K.; Wang, Y. H.; Cai, C. Z.; Lin, H. W. Activating Room Temperature Long Afterglow of Carbon Dots via Covalent Fixation. *Chem. Mater.* **2017**, *29*, 4866−4873.

(14) Chen, Y. H.; He, J. L.; Hu, C. F.; Zhang, H. R.; Lei, B. F.; Liu, Y. L. Room Temperature Phosphorescence from Moisture-resistant and Oxygen-barred Carbon Dot Aggregates. *J. Mater. Chem. C* **2017**, *5*, 6243−6250.

(15) Jiang, K.; Zhang, L.; Lu, J. F.; Xu, C. X.; Cai, C. Z.; Lin, H. W. Triple-Mode Emission of Carbon Dots: Applications for Advanced Anti-Counterfeiting. *Angew. Chem., Int. Ed.* **2016**, *55*, 7231−7235.

(16) Dong, X. W.; Wei, L. M.; Su, Y. J.; Li, Z. L.; Geng, H. J.; Yang, C.; Zhang, Y. F. Efficient Long Lifetime Room Temperature Phosphorescence of Carbon Dots in a Potash Alum Matrix. *J. Mater. Chem. C* **2015**, *3*, 2798−2801.

DOI: 10.1021/acscentsci.8b00844
ACS Cent. Sci. 2019, 5, 349−356

(17) Tan, J.; Zou, R.; Zhang, J.; Li, W.; Zhang, L. Q.; Yue, D. M. Large-scale Synthesis of N-doped Carbon Quantum Dots and Their Phosphorescence Properties in a Polyurethane Matrix. *Nanoscale* **2016**, *8*, 4742−4747.
(18) Li, Q. J.; Zhou, M.; Yang, Q. F.; Wu, Q.; Shi, J.; Gong, A. H.; Yang, M. Y. Efficient Room-Temperature Phosphorescence from Nitrogen-Doped Carbon Dots in Composite Matrices. *Chem. Mater.* **2016**, *28*, 8221−8227.
(19) Gao, Y. F.; Han, H.; Lu, W. J.; Jiao, Y.; Liu, Y.; Gong, X. J.; Xian, M.; Shuang, S. M.; Dong, C. Matrix-Free and Highly Efficient Room-Temperature Phosphorescence of Nitrogen-Doped Carbon Dots. *Langmuir* **2018**, *34*, 12845−12852.
(20) Li, Q. J.; Zhou, M.; Yang, M. Y.; Yang, Q. F.; Zhang, Z. X.; Shi, J. Induction of Long-lived Room Temperature Phosphorescence of Carbon Dots by Water in Hydrogen-bonded Matrices. *Nat. Commun.* **2018**, *9*, 734−742.
(21) Tian, Z.; Li, D.; Ushakova, E. V.; Maslov, V. G.; Zhou, D.; Jing, P. T.; Shen, D. Z.; Qu, S. N.; Rogach, A. L. Multilevel Data Encryption Using Thermal-Treatment Controlled Room Temperature Phosphorescence of Carbon Dot/Polyvinylalcohol Composites. *Adv. Sci.* **2018**, *5*, 1800795.
(22) Xiang, H. F.; Cheng, J. H.; Ma, X. F.; Zhou, X. G.; Chruma, J. J. Near-infrared Phosphorescence: Materials and Applications. *Chem. Soc. Rev.* **2013**, *42*, 6128−6185.
(23) Yu, Z. Y.; Wu, Y. S.; Xiao, L.; Chen, J. W.; Liao, Q.; Yao, J. N.; Fu, H. B. Organic Phosphorescence Nanowire Lasers. *J. Am. Chem. Soc.* **2017**, *139*, 6376−6381.
(24) Xiang, H. F.; Zhou, L.; Feng, Y.; Cheng, J. H.; Wu, D.; Zhou, X. G. Tunable Fluorescent/Phosphorescent Platinum (II) Porphyrin−Fluorene Copolymers for Ratiometric Dual Emissive Oxygen Sensing. *Inorg. Chem.* **2012**, *51*, 5208−5212.
(25) Carlson, B.; Phelan, G. D.; Kaminsky, W.; Dalton, L.; Jiang, X. Z.; Liu, S.; Jen, A. K. Y. Divalent Osmium Complexes: Synthesis, Characterization, Strong Red Phosphorescence, and Electrophosphorescence. *J. Am. Chem. Soc.* **2002**, *124*, 14162−14172.
(26) Zhang, K. Y.; Gao, P. L.; Sun, G. L.; Zhang, T. W.; Li, X. L.; Liu, S. J.; Zhao, Q.; Lo, K. K. W.; Huang, W. Dual-Phosphorescent Iridium (III) Complexes Extending Oxygen Sensing from Hypoxia to Hyperoxia. *J. Am. Chem. Soc.* **2018**, *140*, 7827−7834.
(27) Bhattacharjee, I.; Acharya, N.; Karmakar, S.; Ray, D. Room-Temperature Orange-Red Phosphorescence by Way of Intermolecular Charge Transfer in Single-Component Phenoxazine−Quinoline Conjugates and Chemical Sensing. *J. Phys. Chem. C* **2018**, *122*, 21589−21597.
(28) Zhang, J.; Zhao, F. C.; Zhu, X. J.; Wong, W. K.; Ma, D. G.; Wong, W. Y. New Phosphorescent Platinum (II) Schiff Base Complexes for PHOLED Applications. *J. Mater. Chem.* **2012**, *22*, 16448−16457.
(29) Kui, S. C. F.; Chui, S. S. Y.; Che, C. M.; Zhu, N. Y. Structures, Photoluminescence, and Reversible Vapoluminescence Properties of Neutral Platinum (II) Complexes Containing Extended π-Conjugated Cyclometalated Ligands. *J. Am. Chem. Soc.* **2006**, *128*, 8297−8309.
(30) Chan, K. H. Y.; Chow, H. S.; Wong, K. M. C.; Yeung, M. C. L.; Yam, V. W. W. Towards Thermochromic and Thermoresponsive Near-infrared (NIR) Luminescent Molecular Materials Through the Modulation of Inter- and/or Intramolecular Pt···Pt and $\pi-\pi$ Interactions. *Chem. Sci.* **2010**, *1*, 477−482.
(31) Tanaka, Y.; Wong, K. M. C.; Yam, V. W. W. Phosphorescent Molecular Tweezers Based on Alkynylplatinum(II) Terpyridine System: Turning on of NIR Emission via Heterologous Pt···M Interactions (M = Pt II, Pd II, Au III and Au I). *Chem. Sci.* **2012**, *3*, 1185−1191.
(32) Liu, J. C.; Wang, N.; Yu, Y.; Yan, Y.; Zhang, H. Y.; Li, J. Y.; Yu, J. H. Carbon Dots in Zeolites: A New Class of Thermally Activated Delayed Fluorescence Materials with Ultralong Lifetimes. *Sci. Adv.* **2017**, *3*, No. e1603171.
(33) Pei, X. Y.; Xiong, D. Z.; Wang, H. Y.; Gao, S. Q.; Zhang, X. Y.; Zhang, S. J.; Wang, J. J. Reversible Phase Transfer of Carbon Dots between an Organic Phase and Aqueous Solution Triggered by CO_2. *Angew. Chem., Int. Ed.* **2018**, *57*, 3687−3691.
(34) Wang, B. L.; Mu, Y.; Zhang, C. H.; Li, J. Y. Blue Photoluminescent Carbon Nanodots Prepared from Zeolite as Efficient Sensors for Picric Acid Detection. *Sens. Actuators, B* **2017**, *253*, 911−917.
(35) Wang, B. L.; Mu, Y.; Yin, H.; Yang, Z. Q.; Shi, Y.; Li, J. Y. Formation and Origin of Multicenter Photoluminescence in Zeolite-based Carbogenic Nanodots. *Nanoscale* **2018**, *10*, 10650−10656.
(36) Liu, C.; Xiao, G. J.; Yang, M. L.; Zou, B.; Zhang, Z. L.; Pang, D. W. Mechanofluorochromic Carbon Nanodots: Controllable Pressure-Triggered Blue and Red Shifted Photoluminescence. *Angew. Chem., Int. Ed.* **2018**, *57*, 1893−1897.
(37) Liu, J. J.; Li, D. W.; Zhang, K.; Yang, M. X.; Sun, H. C.; Yang, B. One Step Hydrothermal Synthesis of Nitrogen-Doped Conjugated Carbonized Polymer Dots with 31% Efficient Red Emission for In Vivo Imaging. *Small* **2018**, *14*, 1703919.
(38) Ji, T. J.; Guo, B.; Liu, F. Y.; Zeng, Q. S.; Yu, C. Z.; Du, X. H.; Jin, G.; Feng, T. L.; Zhu, S. J.; Li, F. H.; Yang, B. Cathode and Anode Interlayers Based on Polymer Carbon Dots via Work Function Regulation for Efficient Polymer Solar Cells. *Adv. Mater. Interfaces* **2018**, *5*, 1701519.
(39) Feng, T. L.; Zeng, Q. S.; Lu, S. Y.; Yan, X. J.; Liu, J. J.; Tao, S. Y.; Yang, M. X.; Yang, B. Color-Tunable Carbon Dots Possessing Solid-State Emission for Full-Color Light-Emitting Diodes Applications. *ACS Photonics* **2018**, *5*, 502−510.
(40) Ehrat, F.; Bhattacharyya, S.; Schneider, J.; Lof, A.; Wyrwich, R.; Rogach, A. L.; Stolarczyk, J. K.; Urban, A. S.; Feldmann, J. Tracking the Source of Carbon Dot Photoluminescence: Aromatic Domains versus Molecular Fluorophores. *Nano Lett.* **2017**, *17*, 7710−7716.
(41) Gao, F.; Ma, S. Y.; Li, J.; Dai, K.; Xiao, X. C.; Zhao, D.; Gong, W. F. Rational Design of High-quality Citric Acid-derived Carbon dots by Selecting Efficient Chemical Structure Motifs. *Carbon* **2017**, *112*, 131−141.
(42) Jiang, K.; Wang, Y. H.; Cai, C. Z.; Lin, H. W. Conversion of Carbon Dots from Fluorescence to Ultralong Room-Temperature Phosphorescence by Heating for Security Applications. *Adv. Mater.* **2018**, *30*, 1800783.
(43) Ye, S.; Sun, J. Y.; Han, Y. H.; Zhou, Y. Y.; Zhang, Q. Y. Confining Mn^{2+}-Doped Lead Halide Perovskite in Zeolite-Y as Ultrastable Orange-Red Phosphor Composites for White Light-Emitting Diodes. *ACS Appl. Mater. Interfaces* **2018**, *10*, 24656.
(44) Liu, H. W.; Wu, Z. N.; Shao, J. R.; Yao, D.; Gao, H.; Liu, Y.; Yu, W. L.; Zhang, H.; Yang, B. $CsPb_xMn_{1-x}Cl_3$ Perovskite Quantum Dots with High Mn Substitution Ratio. *ACS Nano* **2017**, *11*, 2239−2247.
(45) Parobek, D.; Roman, B. J.; Dong, Y. T.; Jin, H.; Lee, E.; Sheldon, M.; Son, D. H. Exciton-to-Dopant Energy Transfer in Mn-Doped Cesium Lead Halide Perovskite Nanocrystals. *Nano Lett.* **2016**, *16*, 7376−7380.
(46) Rossi, D.; Parobek, D.; Dong, Y. T.; Son, D. H. Dynamics of Exciton−Mn Energy Transfer in Mn-Doped $CsPbCl_3$ Perovskite Nanocrystals. *J. Phys. Chem. C* **2017**, *121*, 17143−17149.
(47) Scholes, G. D.; Fleming, G. R.; Olaya-Castro, A.; van Grondelle, R. Lessons from Nature about Solar Light Harvesting. *Nat. Chem.* **2011**, *3*, 763−774.
(48) Sun, M. J.; Zhong, Y. W.; Yao, J. N. Thermal-Responsive Phosphorescent Nanoamplifiers Assembled from Two Metallophosphors. *Angew. Chem., Int. Ed.* **2018**, *57*, 7820−7825.
(49) Chen, P. Z.; Weng, Y. X.; Niu, L. Y.; Chen, Y. Z.; Wu, L. Z.; Tung, C. H.; Yang, Q. Z. Light Harvesting Systems Based on Organic Nanocrystals To Mimic Chlorosomes. *Angew. Chem., Int. Ed.* **2016**, *55*, 2759−2763.
(50) Liu, Y. N.; Jin, J. Y.; Deng, H. P.; Li, K.; Zheng, Y. L.; Yu, C. Y.; Zhou, Y. F. Protein-Framed Multi-Porphyrin Micelles for a Hybrid Natural-Artificial Light-Harvesting Nanosystem. *Angew. Chem., Int. Ed.* **2016**, *55*, 7952−7957.
(51) Parkinson, P.; Knappke, C. E. I.; Kamonsutthipaijit, N.; Sirithip, K.; Matichak, J. D.; Anderson, H. L.; Herz, L. M. Ultrafast Energy

DOI: 10.1021/acscentsci.8b00844
ACS Cent. Sci. 2019, 5, 349−356

Transfer in Biomimetic Multistrand Nanorings. *J. Am. Chem. Soc.* **2014**, *136*, 8217−8220.
(52) Vijayakumar, C.; Praveen, V. K.; Kartha, K. K.; Ajayaghosh, A. Excitation Energy Migration in Oligo(p-phenylenevinylene) based Organogels: Structure-property Relationship and FRET Efficiency. *Phys. Chem. Chem. Phys.* **2011**, *13*, 4942−4949.

DOI: 10.1021/acscentsci.8b00844
ACS Cent. Sci. 2019, 5, 349−356